Supporting Information

# Charge Trapping and Exciton Dynamics in Large-area CVD Grown $MoS_2$

Paul D. Cunningham,[1*] Kathleen M. McCreary,[1] Aubrey T. Hanbicki,[1] Marc Currie,[1] Berend T. Jonker,[1] and L. Michael Hayden[2,†]

## Modeling of transient absorption spectra

The TA spectrum is modeled as changes in the ground state absorption amplitude, line-width, and center wavelength as described in the main text. It is counter intuitive that a shift in the TA spectrum does not necessarily imply that the absorption spectrum has shifted. Instead, spectral shifts of the absorption features cause an oscillatory TA spectrum that changes sign depending on the direction of the shift, Figure S1.

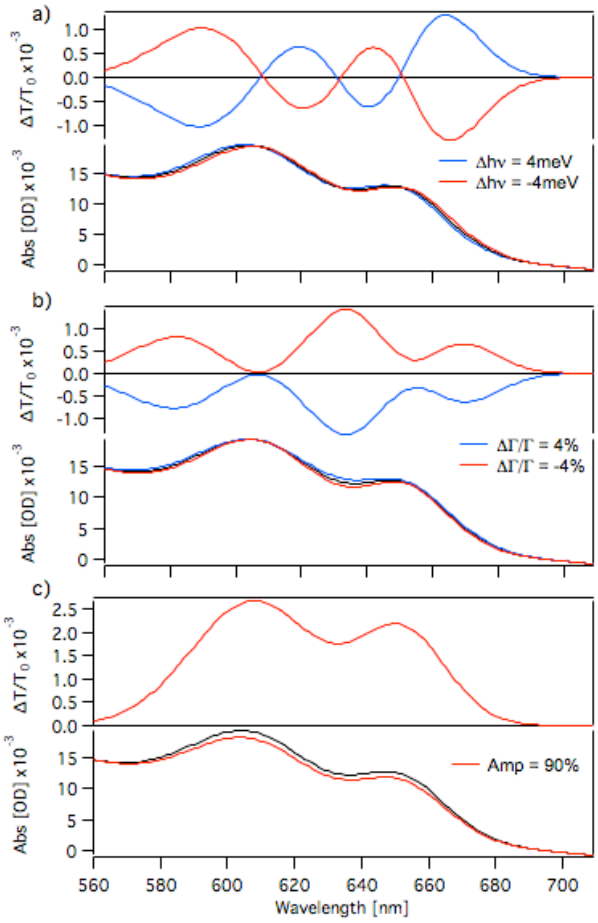


Figure S1. Modeled change in transmission curves show how the TA spectrum would look for changes in the absorption (a) center wavelengths, (b) line-widths, and (c) amplitudes.

The 0th spectral moments of the A and B features,

$$\left\langle A^0(t)\right\rangle = \frac{\int_{\lambda_1}^{\lambda_2}\left(\Delta T/T_0\right)d\lambda}{\lambda_2-\lambda_1}, \qquad \text{(S1)}$$

are simply the average change in transmission across the wavelength region of interest. We find that the 0th spectral moments of the A and B features match the temporal dependence of the line-width broadening, Figure S2, indicating that line-width broadening dominates the TA spectra. Interestingly, the difference between these spectral moments matches the measured red shift dynamics.

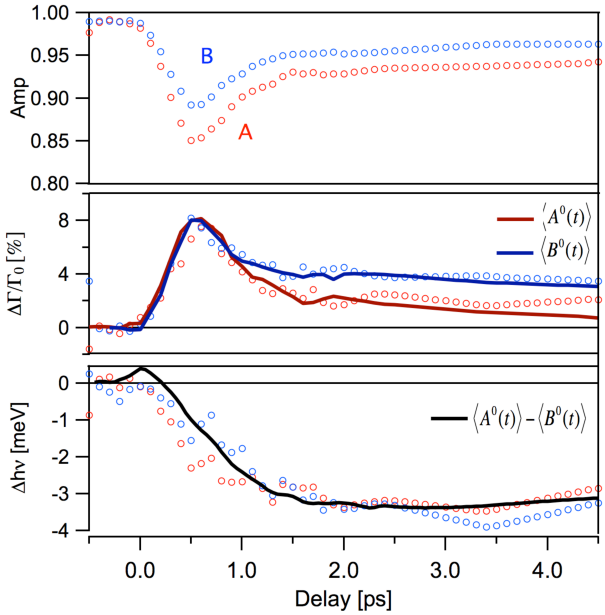


Figure S2. A comparison between the transient absorption fit results in Figure 2d and the 0th spectral moments of the A (red, solid line) and B (blue, solid line) features. The difference between these two spectral moments (black) is also shown.

The observed spectra clearly show a larger change in transmission in the vicinity of the B feature than for the A feature. If interpreted as arising from bleaching alone, such a spectrum would imply that more B excitons are excited, i.e. that holes are in the lower energy spin-orbit split valance band. However the fit parameters show greater occupancy of the A states. This is because broadening and the red-shift of the B feature lead to increased absorption that overlaps with the A feature. This increased absorption means that the change in transmission will be negative. This overlapping negative contribution from the B exciton caused the A feature to appear lower in amplitude, Figure S3.

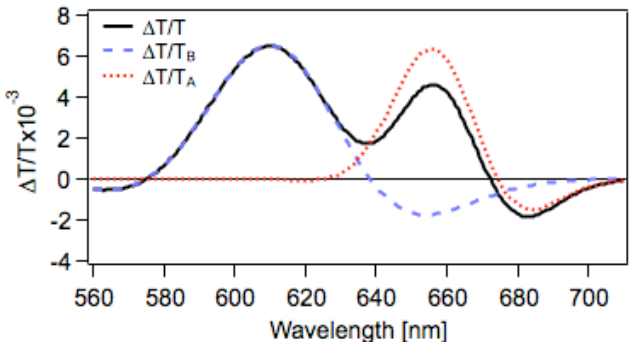


Figure S3. The modeled change in transmission (black) can be separated into contributions from the A (red) and B (blue) excitons.

**Fluence dependence of the transient absorption spectra**

The transient absorption spectra shows an apparent red-shift with increasing fluence. Applying our model to fluence-dependent TA spectra resulting from 387 nm excitation reveals that both the line-width broadening and the red-shift increases to produce this apparent shift, Figure S4. Though counterintuitive, this is not unexpected since a red-shift in the absorption does not produce a red-shift in the TA spectrum but instead produces an oscillatory spectrum, whose sign and amplitude depend on the direction and magnitude of the spectral shift.

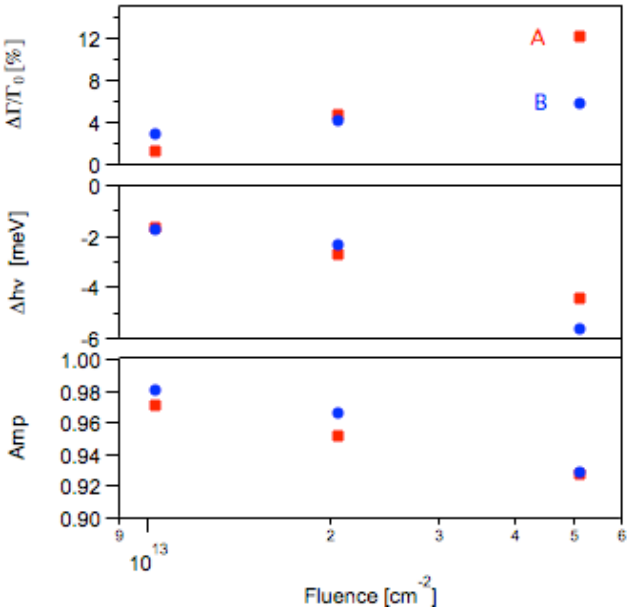


Figure S4. The modeled change in line-width, center wavelength, and amplitude as a function of fluence for 387 nm excitation of monolayer $MoS_2$.

**Excitation photon energy dependence of the transient absorption spectra**

The transient absorption spectra are essentially independent of excitation wavelength. A comparison between TA spectra for 387 nm, 532 nm, and 775 nm excitation wavelengths all show qualitatively the same behavior, Figure S5. Choosing specific probe wavelengths, we see that neither the slow, Figure 4d, nor the fast, Figure S6, component varies with excitation wavelength.

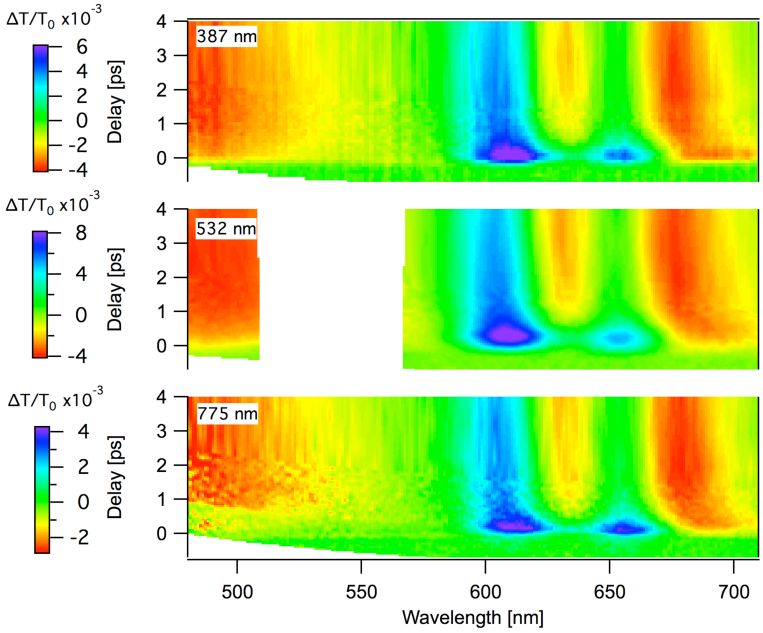


Figure S5. Transient absorption spectra measured as a function of delay for monolayer $MoS_2$ photo-excited at (a) 387 nm, (b) 532 nm, and (c) 775 nm.

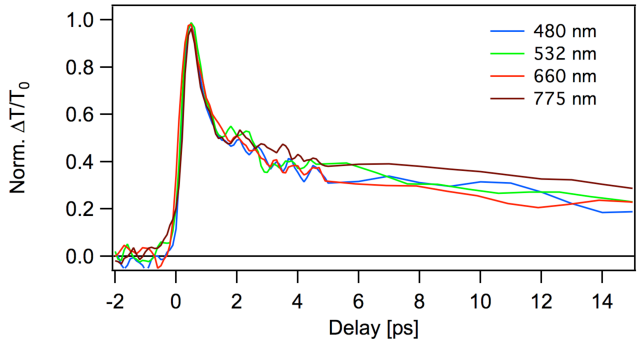


Figure S6. The excited state dynamics of monolayer $MoS_2$ measured at a probe wavelength of 610 nm for excitation wavelengths of 480 nm, 532 nm, 660 nm, and 775 nm.

**Substrate and film thickness dependence**

The photoconductivity and excited state dynamics were measured for $MoS_2$ films on three different substrates: TOPAS® polymer, sapphire, and fused-silica, Figure S7. These substrates were selected for their low absorption at THz frequencies. Silicon could not be used as a substrate because the photoconductivity response would dwarf that observed in $MoS_2$. We see no significant change in the dynamics among these different substrates. It is also worth mentioning that the decay observed in the photoconductivity and the sub-picosecond decay component of the excited state dynamics both appear to be largely unaffected by film thickness, Figure S8. This is unexpected and these results seem inconsistent with either a surface or interface trapping mechanism.

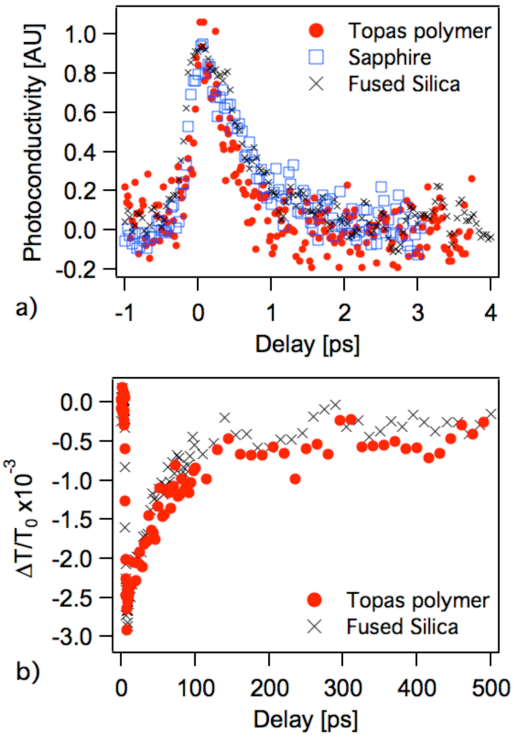


Figure S7. The (a) photoconductivity dynamics and (b) excited state dynamics of monolayer $MoS_2$ probed at 480 nm on TOPAS® polymer (red circles), sapphire (blue squares), and fused silica (black x). The sapphire was single-side polished and could not be used for transmission experiments at optical wavelengths due to scattering losses.

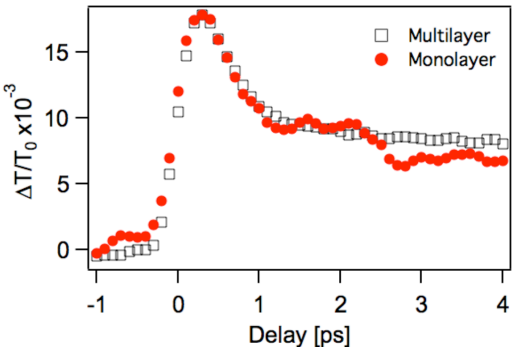


Figure S8. The excited state dynamics probed at 610 nm for mono- (red circles) and multilayer (black squares) $MoS_2$.

## Temperature dependence

We mounted $MoS_2$ films in a closed-cycle liquid helium cooled optical cryostat outfitted with TOPAS® polymer windows. The photoconductivity was measured at room temperature and at 15K via TRTS. No significant change in the dynamics was observed, Figure S9.

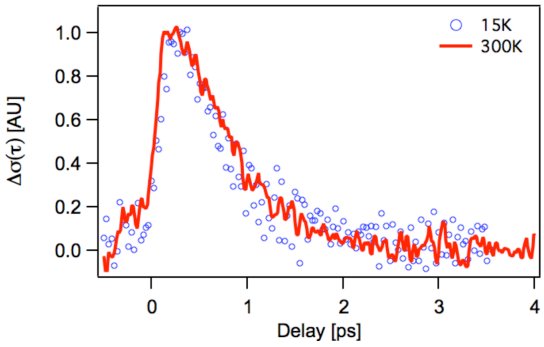


Figure S9. Photoconductivity dynamics in monolayer $MoS_2$ measured via TRTS at 300K and 15K.

## Comparison of different sample preparation techniques

To evaluate the quality of our CVD grown $MoS_2$ monolayer films, photoluminescence (PL) was measured for the three different sample preparation methods in Figure S10: a mechanically exfoliated monolayer, CVD growth using $MoCl_5$ as a precursor, and CVD growth using $MoO_3$ as a precursor. CVD growth of monolayer $MoS_2$ using $MoCl_5$ as a precursor results in uniform large area polycrystalline films with grain sizes of approximately 10 nm.[9, 10] The high density of grain boundaries or defects present in the film leads to the lowest luminescence intensity and largest full-width at half-maximum (FWHM). By comparison, the luminescence in Figure 1c was recorded at higher excitation intensity and with a longer integration time. Exfoliated flakes of $MoS_2$ are typically 1 μm in

size and presumed to be single crystalline. However, bulk $MoS_2$ is known to contain C and O impurities,[7] which may contribute to the only modest improvement in luminescence intensity and narrowing of FWHM. CVD growth using $MoO_3$ as a precursor results in less uniform films consisting of large equilateral triangle grains of order 10 μm.[9] These films exhibit a dramatic enhancement in luminescence intensity and narrower FWHM. This comparison suggests that defect densities and grain boundary densities are correlated.

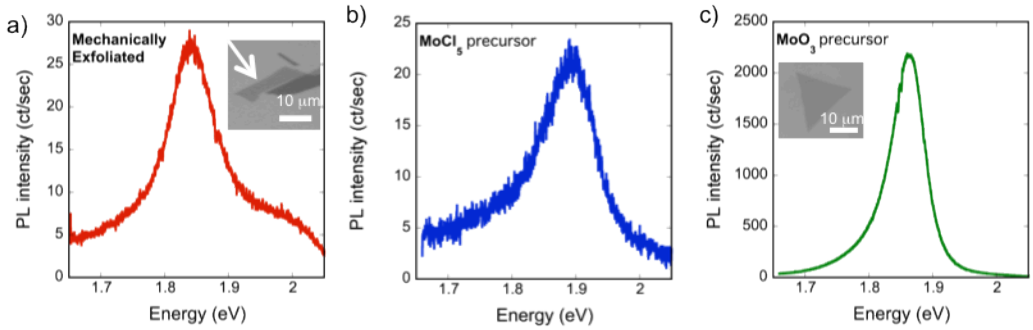


Figure S10. Photoluminescence from monolayer $MoS_2$ films prepared via (a) mechanical exfoliation, (b) CVD growth using $MoCl_5$ precursor, and (c) CVD growth using $MoO_3$ precursor.